The Thesis Committee for Varun Pattani
Certifies that this is the approved version of the following thesis:

Nanoparticle-mediated photothermal therapy of tumors: A comparative study of heating efficiencies for different particle types

APPROVED BY
SUPERVISING COMMITTEE:

Supervisor:

James W. Tunnell

Pengyu Ren

Nanoparticle-mediated photothermal therapy of tumors: A comparative study of heating efficiencies for different particle types

by

Varun Paresh Pattani, B.S.

Thesis

Presented to the Faculty of the Graduate School of

The University of Texas at Austin

in Partial Fulfillment

of the Requirements

for the Degree of

Master of Science in Engineering

The University of Texas at Austin

May 2010

Acknowledgements

I would like to thank my family including my sister, Kiran Pattani, my mother, Kalyani Pattani, and my father, Paresh Pattani. I appreciate their support and love throughout the years from my time in pre-school to now in finishing my Master's degree.

I would also like to thank my friends from high school and Cornell to here at the University of Texas for their support, advice and most of all for keeping things in perspective.

I would like to thank all of my colleagues in the Biophotonics Lab for their help and advice throughout. Additionally, I would like to acknowledge our collaborators, the team at Nanospectra Biosciences Inc., for their support in providing the nanoparticles and biofunctionalization.

Finally, I would also like to thank my supervisor, Dr. James W. Tunnell, for his incredible guidance and support during this project.

Abstract

Nanoparticle-mediated photothermal therapy of tumors: A comparative study of heating efficiencies for different particle types

Varun Paresh Pattani, M.S.E.

The University of Texas at Austin, 2010

Supervisor: James W. Tunnell

Cancer is one of the most notorious diseases affecting the human population today with very few effective treatments. Due to the disparate nature of cancers, it is difficult to obtain a treatment that can cure cancer. Thus, there is a large influx of research towards cancer therapies, leading to one of the discovery that cancer cells (tumors) have a low thermotolerance in comparison to normal cells. If the temperature of the cancer cells is increased into the hyperthermia range (~45°C) thermal damage occurs, causing cell death by protein denaturation and membrane disruption. A recent development in this field has been in the photothermal treatment of tumors, which is starting to utilize

plasmonic particles to enhance the specificity of the treatment. The plasmonic nanoparticles, specifically gold, can reach the tumor site using passive targeting and when irradiated with a tuned laser will emit heat localized to a small region around the nanoparticle killing the surrounding cancer cells. This process has been shown to reduce tumor size *in vivo* with gold nanoshells and gold nanorods.

However, it has not been shown which particle is better at delivering the heat to the tumor site. Therefore in this study, it will be shown which particle generates the most heat. Solutions of tissue simulating phantom and different concentrations of nanoparticles were irradiated with a laser to measure the increase in temperature. Additionally, simulations were performed using Mie Theory for nanoshells and the Discrete Dipole Approximation for nanorods. Based on the physical parameters of the nanoshells and nanorods used in this experiment, the adjusted absorption cross-section was determined. It was found that nanoshells generated the most amount of heat on a per particle basis, and that it was necessary to have a nanorod concentration of 5.5 times the concentration of nanoshells to generate the same amount of heat as nanoshells. These results were confirmed using Monte Carlo and Finite Difference Modeling of the nanoparticle heating experiments. However, the choice of nanoparticle still depends on the application and the targeting efficiency *in vivo*.

Table of Contents

List of Tables

List of Figures

INTRODUCTION

1.1 Cancer, General

Cancer is a disease that affects approximately 12 million people each year and consistently leads to a reduction in the quality of life if not death. Because this disease is based on mutations in the DNA encoding normal cellular proteins, each type of cancer is very different. For this reason, there has been no perfect method to treat all forms of cancer. Additionally, it has been found that cancer forms in a multi-step process that usually progresses over many years, thus making it hard to detect when it occurs. This also makes it hard to treat because it is not always possible to find the cause of the cancer as well as the primary organ in metastatic cancers. (1-2)

The acquired capabilities of most cancers can be divided into six main categories: [1] self-sufficiency in growth signals, [2] insensitivity to anti-growth signals, [3] tissue invasion and metastasis, [4] limitless replicative potential, [5] sustained angiogenesis, and [6] evading apoptosis. The first acquired capability, self-sufficiency in growth signals, states that these cancer cells have developed the ability to replicate without the need of mitogenic stimuli. Secondly, these cancer cells have developed the ability to grow even in the presence of proteins that, in normal cells, stop proliferation. The third capability states that these cancer cells have the ability to travel through the lymphatic and circulatory systems and move into other organs and increase proliferation and create new tumor masses throughout the body. Fourthly, these cancer cells have the transformed ability to continue proliferating well after the predicted cell lifetime. Fifth, is that these cancer cells release large amounts of angiogenic growth factors, such as VEG-F, to

branch off new vasculature to the tumor site thus increasing the tumor self-sufficiency. Finally, these cancer cells have the ability to evade apoptosis, programmed cell death, leading to immortalization of these cells due to the fact that there are mutations that affect such pathways as the p53 and Rb pathways. (3)

1.2 Cancer Treatment

With so many steps and cellular pathways involved in the development of cancer, there is no effective way to treat all cancers successfully. Approved treatments being used in oncology today include surgery, chemotherapy and radiation therapy. Surgery is the oldest practice that has been used and the most efficient because the cancer cells are removed and cannot proliferate any more within the tissue. However, the main limitation is that it is not always possible to delineate the margins of the tumor, possibly leaving cancer initiating cells. Additionally, if invasion and metastasis has started to occur there may be multiple tumors and tumor cells in the circulatory or lymphatic system. Both chemotherapy and radiation therapy target all highly proliferating cells within the body , thus not only cancer cells are targeted but also such cells as hair follicles, gastrointestinal epithelium, and immune cells. These processes work on first-order kinetics in that only a fraction of the cancer cells are killed during each treatment. Since these treatments are also very toxic to the human body, there also needs to be an upper limit to the amount of treatments performed. Radiation therapy is relatively localized; however, chemotherapy is systemic and affects the whole body.(4-6) The need for early detection of cancer, for easier as well as better treatments of cancer is readily apparent. As such, the

investigation for a minimally invasive, non-surgical, method of cancer therapy is currently a widely researched topic.

1.3 Thermal Therapy

One potential solution involves delivering heat to the tumor site. Heat has been used to treat tumors for many years ranging back to 1700 BC, however, it was recently discovered that there is a correlation between tumor cells dying in response to heat. Tumor cancer cells were found to be thermally sensitive due to their reduced heat tolerance because of the poor blood supply.(7-8) Even with sustained angiogenesis the vasculature in cancerous tumors is very irregular.(9) Thus, one technique being explored for cancer therapy is a hyperthermia-based procedure, thermal therapy, in which diseased tissue is heated to high temperatures in the hyperthermia regime (ranging from 42-47° C) which results in cell death. (10-11)

Many techniques of delivering this heat to tumor have been utilized to increase the temperature in the tumor site into the hyperthermia regime. The possible modalities can range from radio-frequency (RF), both capacitative and electromagnetic heating, to microwave heating and also ultrasound heating.(12-15) Capacitative RF heating works by creating a circuit with the region of interest, which leads to heating in that part of the body, but it's limited because there is preferential heating in fatty tissue. Another method used to heat tumors is by inducing eddy currents using alternating magnetic fields, yet this leads to the surface temperature increasing higher than desired. There has been a general trend of movement towards microwave heating using interstitial antennas in the

434 and 915 MHz range, which has higher penetration and better heating profiles.(16) However, these modalities are still limited due to their lack of specificity in delivering heat to only the tumor site without cutting into the patient. The surrounding healthy tissue is also damaged when the tumor site temperature was increased. Consequently, there is a desire for having a technique that delivers heat specifically targeted to only the cancerous tumor and without affecting the surrounding tissue.

1.4 Photothermal Therapy

A more targeted approach to cancer hyperthermia therapy, which directly targets the heat to the tumor, is a process known as photothermal therapy. It is a therapeutic process by which electromagnetic radiation, in this case, light, is converted into thermal energy using a photosensitive probe. When irradiated with light, the electrons in these photosensitive probes jump from the steady state into an excited state and relax through non-radiative decay processes resulting in kinetic energy changes creating localized heat.(17) These probes include cellular chromophores that absorb strongly at certain wavelengths or they can be externally injected dye molecules such as indocyanine green.(18-19) The natural chromophores are ineffective at converting light into heat, which makes it difficult to heat tissue at low laser powers. Externally injected dye molecules are limited by their photobleaching effect when irradiated with a laser. Thus, there is a need for an exogenous photothermal agent that has high optical absorption cross-sections, as well as being efficient at converting the incident light into heat, making the therapy less invasive due to lower incident laser powers. Noble metal

nanoparticles have been shown to be photothermally active, killing cancer cells *in vitro* and reducing tumor size dramatically *in vivo*. (20-25)

1.5 Nanoparticles

One promising molecularly specific targeted therapy uses nanovectors, nano-sized particles with multiple functions. Nanovectors have been used for three main functions: [1] imaging, [2] targeting, [3] and therapy. One example nanovector includes liposomes, because these lipid structures can be used to encapsulate drugs and deliver them to targets, such as tumor sites. Liposomes have been used with many different cancer related drugs including doxorubicin.(26) Another class of nanovector is known as nanoparticles, which are synthesized particles with a diameter within the nanometer range. Nanoparticles have been composed of many different materials including titanium dioxide, iron oxide (magnetically excited), gold, silver (noble metals – optically excited), and cadmium selenide (semiconductor nanoparticles). An important factor of nanoparticles is that the properties of the materials that make up these nanoparticles change when reduced to the nanoscale. This includes quantum confinement in semiconductor nanoparticles, superparamagnetism in magnetic nanoparticles, and surface plasmon resonance in noble metal nanoparticles.(27-28)

These nanoparticles can act as carriers for these drugs because it is possible biofunctionalize drugs to the particle or encapsulate them within the particle. Additionally, it is possible to target certain biomarkers by conjugating antibodies and other targeting particles such as peptides onto the surface of these nanoparticles.

Targeting is a major factor in nanoparticle synthesis, because all of these nanoparticles have to reach their specific target to fulfill their response. As a result, a concern for nanoparticle targeting is cytotoxicity and clearance time in the bloodstream. Most of these discussed nanoparticles have been shown to not be cytotoxic; however, there are still concerns with the toxicity of the semiconductor nanoparticles. To reduce the cytotoxicity and increase the clearance time the nanoparticle is "stealthed". Poly-ethylene glycol (PEG) is coated on the surface of these nanoparticles to neutralize the surface charge. This stabilizes the nanoparticle and reduces the opsonization process of plasma proteins being deposited on the surface of the foreign agents.

An extremely notable use of these nanoparticles is in cellular and molecular imaging. Colloidal nanoparticles have become important as imaging agents due to their potential noncytotoxic immunotargeting and insusceptibility to denaturation. Each nanoparticle provides a different set of optical behaviors that can be utilized for different imaging techniques. For *in vivo* imaging and therapeutic techniques, near-infrared light (NIR) is the most desired region of the electromagnetic spectrum for high optical resonance. Furthermore, these nanoparticles can be used as imaging agents for many different modalities: fluorescently with semiconductor nanoparticles, using MRI with magnetic nanoparticles, and optical coherence tomography and two photon microscopy with noble metal nanoparticles.(29-35)

1.6 Surface Plasmon Resonance

Gold nanoparticles (GNPs) have the ability to fulfill the requirements necessary to be highly absorbing photosensitive probes for photothermal therapy. This is due to the innate property of noble metals fabricated on the nanoscale, enhanced surface plasmon resonance (SPR). A surface plasmon is the oscillation of electrons on the surface of a material. SPR occurs when these electrons oscillate together in the presence of an electromagnetic field at a specific frequency. This causes the nanoparticles to absorb electromagnetic radiation in resonance with the SPR frequency. When the SPR frequency of a particle can be shifted, the particle is said to be optically tunable. SPR frequency is largely dependent on the geometry of the nanoparticle. Nanosized gold colloids are known to have an SPR frequency in the visible light range with limited tunability due to variations in radius. (37-39)

The strongly enhanced SPR of noble metal nanoparticles at optical frequencies makes them excellent scatterers and absorbers of visible and near-infrared light. Once new methods for biomolecule-nanoparticle conjugates were discovered, the efficacy of nanoparticles for biomedical applications greatly increased. (40-43) Medical diagnostics and therapeutic applications implementing GNPs have not only been successful methods but also biocompatible methods. Therefore, understanding the optical properties of these GNPs becomes essential when attempting to harness all the potential this technology possesses. From electric field data and optical cross-section data, photothermal applications and other optical therapeutic techniques become viable additions to GNP research thrusts.

1.7 Gold Nanoparticles in Photothermal Therapy

Two types of plasmonic GNPs, gold nanoshells and gold nanorods, were compared in this study with regards to their respective heating. Nanoshells are spherical particles with a dielectric core of silica and a metal shell of gold. Nanorods are pill-shaped gold colloids. Both particles have the surface plasmon resonance property due to their gold surfaces. A unique property of both of these GNPs is the ability to tune the resonance peak such that the particle can absorb and scatter light to different points within the spectra. With nanoshells, the peak shifts based on the core to shell diameter ratio, and for the nanorods, the peak shifts based on the aspect ratio, which is the ratio between the length and width. It is beneficial for *in vivo* applications to tune the GNP absorption peak into the near infrared region (NIR, 700–1000 nm), known as the tissue optical window, where light penetration in tissue is largest due to minimal absorption and scattering. (37-38) Due to their small size (~20-100 nm) these GNPs have short relaxation times, which leads to heat being localized only to the immediate surroundings of the nanoparticle.

These GNPs can be designed to accumulate at cancerous tumor sites. The GNPs are systemically injected into the bloodstream (Figure 1A), and use a passive mechanism known as the EPR (enhanced permeability and retention) effect to reach the tumor. The EPR effect is due to newly-formed vasculature within tumor sites, which are "leaky" as a result of nanometer sized pores (~500 nm) through which these GNPs can reach the tumor (Figure 1B). (44) The newly-formed vasculature within tumor sites is "leaky" due to rapid and disorganized tumor angiogenesis.

The gold surfaces are readily bioconjugable, thus cancer biomarkers can be conjugated on the surface of the GNPs to actively target cancerous cells. In many cases, cancer biomarkers have been used to target cancer cells successfully *in vitro*. When attached to these cancerous cells, the photothermal therapy is administered by irradiating the cancer cells with a laser, either pulsed or continuous wave, thus inducing heat from the GNPs, killing the cells through such processes as protein denaturation and cellular membrane disruptions (Figure 1C). (45-46)

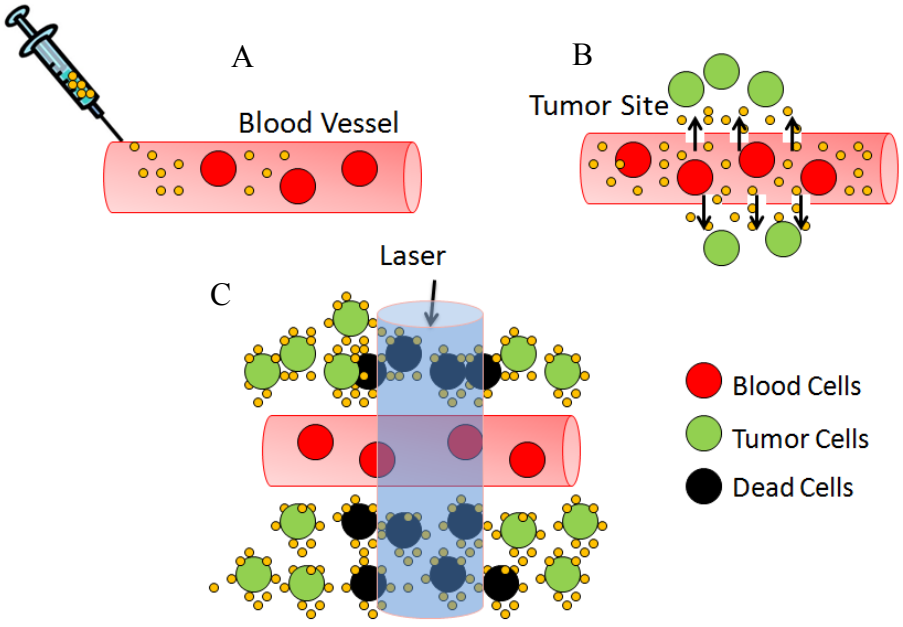

Figure 1: GNP Delivery to Tumor Site. (A) Gold GNPs are injected systemically into the circulatory system, mixing into the blood stream with the red blood cells. At the tumor site (B), using a passive mechanism known as EPR, the GNPs diffuse into the tumor. After a known incubation time, the tumor site is irradiated with a NIR laser (C) to heat the cells to high enough temperatures to induce cell death.

The first experiments using photothermal therapy of cancerous cells, *in vitro*, with GNPs were using gold nanospheres, with a surface plasmon resonance peak in the visible region. One of the first studies was by Pitsillides *et al*, in 2003, where they conjugated 20 and 30 nm gold nanospheres with the CD45 antibody, which is overexpressed in certain lymphocytes, in this case human T lymphocytes. The authors irradiated samples with these nanospheres bound to the lymphocytes with 100 laser pulses (565 nm wavelength, 20 ns duration) at 0.5 J/cm^2 and determined that with 100 GNPs/cell there was 54% lethality and 95% for 500 GNPs/cell. Finally, they found that most of the cell death was necrotic using fluorescent stains that detect early apoptosis and necrosis.(22) That same year Zharov *et al* did similar photothermal studies with pulsed nanosecond laser irradiating gold nanospheres incubated with K562 cancer cells.(47) They found that cavitation bubbles formed during heating around the GNPs could be a primary cause to cell death through membrane disruption. Working on this concept, they continued by amplifying the photothermal process using cavitation bubbles on other cancer cells including colon and breast cancer.(21,48-49)

Through these studies and others, it was found that nanosecond pulsed lasers caused controlled and localized heating to only a nanometers around the GNPs depending on the size of the particles and the pulse duration.(48) This process was favorable for ablating small tumors and single cell killing, but it does not have a high heating efficiency. Therefore continuous wave (CW) laser irradiation can be useful for a wider field of lower temperature heating causing cell death through hyperthermia. El-Sayed *et*

al used CW laser irradiation for *in vitro* gold nanosphere based photothermal therapy. They used 40 nm gold nanospheres conjugated with anti-EGFR antibody, which targets many epithelial cancers that overexpress the epidermal growth factor receptor (EGFR), in this case, squamous cell carcinoma cells. The authors found that cancer cell damage occurred after CW laser irradiation of 4 minutes with an Argon laser (514 nm) with a fluence of 19 W/cm^2. (24)

Gold nanoshells, however, soon become a more widely used GNP for photothermal therapy due to its NIR resonance peak, which can be translated to *in vivo* studies. Hirsch *et al* was the first paper to demonstrate the effectiveness of the gold nanoshell based photothermal therapy *in vitro* and *in vivo*. The authors were able to cause cancer cell damage using PEGylated nanoshells incubated with breast cancer cells and irradiated them with a NIR laser (820 nm) at 35 W/cm^2 for 4 minutes. For *in vivo* studies, the authors used a transmissible venereal tumor model by inoculating these transmissible tumor cells into the hind legs of the mouse. After growing to a large enough size, these nanoshells were directly injected into the tumors and irradiated with the NIR laser for 4 minutes at 4 W/cm^2. They found these tumors reduced in size due to cell damage, shrinkage and coagulation.(20) Continuing on their *in vivo* studies, in their next paper, O'Neal *et al*, the authors inoculated tumor cells into the mouse using subcutaneous injection of murine colon carcinoma cells with a tumor xenograft model. The authors then injected the particles into the tail vein of the mouse and using the process of enhanced permeability and retention effect (EPR) the nanoshells accumulated

into the tumor site. After irradiation with the NIR laser (808 nm) for 3 minutes at 4 W/cm^2 they found that the tumor reduced in size and that the mice looked tumor free and healthy until 90 days after treatment.(50) Enhancing on their *in vitro* study, in Loo et al, the authors conjugated anti-HER2 antibody onto the nanoshells. HER2 is a receptor in EGFR family that is overexpressed in breast cancer cells, in this case SKBr3 breast carcinoma cells. After incubation with different PEGylated and antibody-conjugated nanoshells, the authors found preferential cellular binding with the antibody-conjugated nanoshells. The cells and antibody-conjugated nanoshells were irradiated with an NIR laser (820 nm) for 7 minutes at 0.008 W/cm^2 and complete cancer cell death within the laser spot size was found.(36)

Gold nanorods can also be tuned to have their surface plasmon resonance peak in the NIR, thus, these particles are also being used widely in photothermal therapy studies. The first demonstration of photothermal therapy with gold nanorods was conducted by Huang *et al*.(51) In that paper, the authors conjugated anti-EGFR antibody onto the gold nanorods to be incubated with squamous cell carcinoma cells that overexpress EGFR. Here the authors report preferential binding for antibody-conjugated nanorods by showing that the fluence rate necessary to cause cell death, with a Ti-Sapphire 800 nm CW laser over a 4 minute exposure time, was 20 W/cm^2 for normal cells, which do not overexpress EGFR, and 10 W/cm^2 for carcinoma cells that did overexpress EGFR. This study was continued *in vivo* with PEGylated nanorods (non-targeted) in Dickerson *et al*.(52) In this paper, mice were inoculated with human squamous carcinoma cells

subcutaneously in a tumor xenograft model. The nanorods were injected both directly and through the tail vein taking advantage of the EPR effect. Both sets of experiments were irradiated with the Ti-Sapphire (800 nm) CW laser for 10 minutes, but with varying levels of power. The directly injected nanorods received 0.9-1.1 W/cm^2 and the intravenously injected nanorods received 1.7-1.9 W/cm^2. It was found that during the 13 day observation period, after irradiation, all of the tumors had inhibited growth and there was resorption in >57% of the tumors for directly injected nanorods and 25% of the tumors for the intravenously injected nanorods.

Another group, Takahashi *et al*, has also done photothermal studies with nanorods. The authors report using a pulsed NIR laser (1064 nm with a pulse duration of 5-7 ns and repetition rate of 10 Hz) to irradiate HeLa cells incubated with gold nanorods. They found cell death and also report that repeated pulses cause the gold nanorods to melt and deform into spherical particles, which do not absorb strongly in the NIR.(53-54)

One group, Lu *et al*, has looked at targeted photothermal therapy *in vivo* with hollow gold nanoshells with a resonance peak in the NIR. These hollow gold nanoshells were conjugated with a melanocyte stimulating hormone (MSH) which preferentially binds to malignant melanoma cells that overexpress melanocortin type-1 receptor. The malignant melanoma cells were subcutaneously injected into mice using the tumor xenograft model. The authors found that *in vivo*, there was a significant difference between tumor uptake of MSH conjugated hollow nanoshells and PEGylated hollow nanoshells, on the order of ~7 times as many. Additionally, the authors found that the

energy required to have successful photothermal therapy *in vivo* with the targeted nanoshells was 0.5 W/cm^2 for 1 minute at 808 nm wavelength. (55)

1.8 Differences in Gold Nanoshells and Gold Nanorods

There are major differences between the two GNPs of interest, specifically the disparity in the size and shape. Nanoshells, which are composed of a silica core and gold shell, (Figure 2A) have different optical properties than gold colloids, such as gold nanospheres. Nanoshells are usually larger in size; hence, the optical absorption cross-section of nanoshells is significantly more than in nanorods per particle. Therefore, the nanoshells absorb more light based on surface area. Conversely, nanorods, which are smaller, have a higher optical absorption efficiency per particle leading to the notion that these GNPs should absorb the incident light at a higher rate than nanoshells.(38)

Due to its pill shape, gold nanorods can have surface plasmons in the longitudinal and transverse directions. This allows for two SPR frequencies and therefore two absorption peaks. The first peak is due to the transverse SPR frequency in the visible light range and is relatively untunable. The second peak is due to the longitudinal SPR frequency in the near-infrared range and can be easily shifted by changes in the aspect ratio of the nanorods in solution. It is the high optical tunability of this peak that makes gold nanorods so biomedically applicable. Therefore, the absorption efficiency, and consequently the heating efficiency, depends strongly on the polarization of the light and the orientation of the nanorods (Figure 2B). (38,56-57)

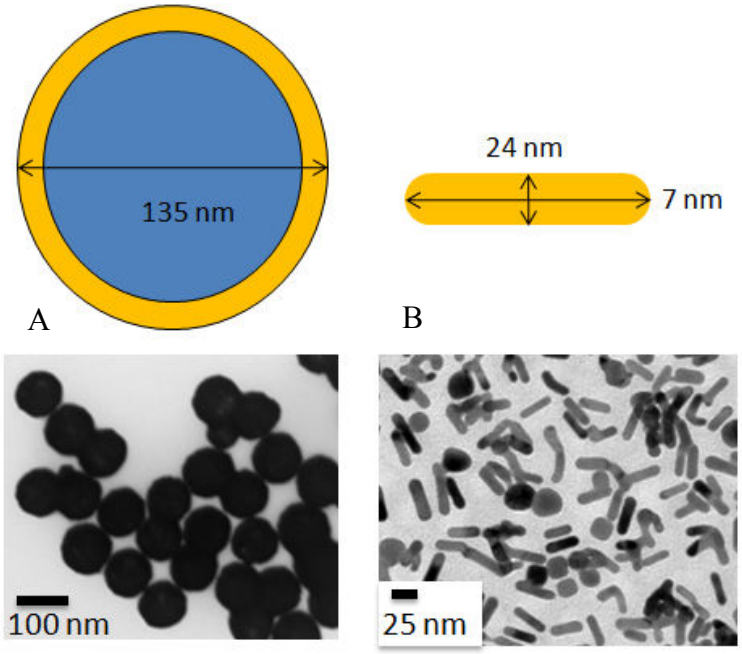

Figure 2: Physical Properties of Nanoshells and Nanorods. (A) Nanoshell size and shape of core plus shell as well as TEM images of these nanoshells. (B) Nanorod size and shape with dimensions as well as TEM images of the nanorods.

1.9 Objectives

The purpose of this study is to compare the ability of nanoshells and nanorods to convert light into heat in a tumor-simulating environment. In this study, Discrete Dipole Approximation (DDA) is used to simulate nanorod absorption in conjunction with experimentation; the difference in heating of randomly oriented nanorods will be shown. Additionally, Mie Theory will be used to determine the optimal scattering and absorption properties of nanoshells. An infrared camera was used to measure the surface temperature of tissue simulating phantoms. With this information it is possible to get the best estimate of the heating by modeling the experiments with Monte Carlo and Finite

Difference Modeling. There needs to be a differentiation between the optical efficiencies and photothermal efficiencies as well as determining the particles efficacy per particle and in concentration. Additionally, the concentration of nanorods will be determined to achieve the same heating as the physiological dose of nanoshells, as found in other biodistribution studies.(58-59)

The final goal of this project is to determine the attributes of both particle types for photothermal therapy. While this GNP-mediated photothermal therapy is effective with various GNPs, the photothermal heating efficiency, in concentration, depends on physical attributes including shape, size, orientation, and GNP aggregation.

METHODS

2.1 Nanoparticle Fabrication

Nanoshell and nanorod solutions were provided by Nanospectra Biosciences, Inc (Houston, TX). The fabrication process for both nanoparticles has been discussed in detail previously.(39,60) The nanoshells, tuned to an absorption peak at 813 nm (Figure 3), have a total radius of 67.5 nm, with a silica core radius of 60 nm and a gold shell thickness of 7.5 nm (Figure 2A). The nanorods were 23.5 nm in length and 7.3 nm in width, leading to an aspect ratio of 3.2 and an effective radius of 8.7 nm (Figure 2B). Additionally, the nanorods were tuned to have an absorption peak at 790 nm (Figure 3). Both GNPs were conjugated with PEG to best mimic the GNPs that are used *in vitro* and *in vivo* due to their "stealthing" properties discussed earlier in this study.

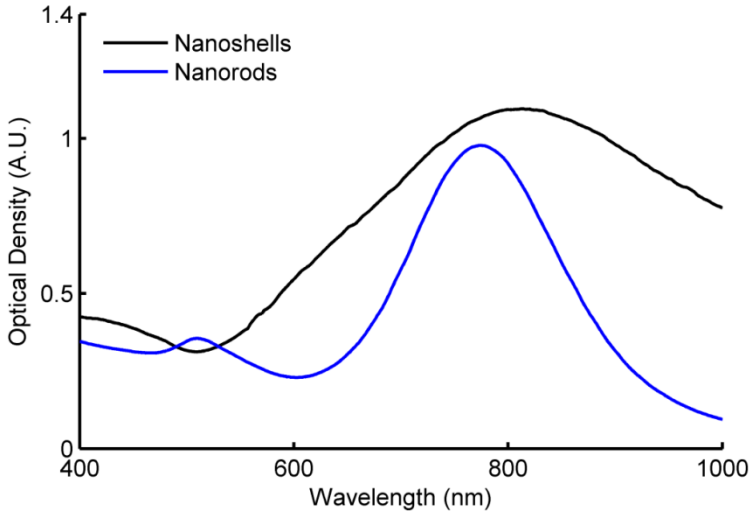

Figure 3: Absorption spectra. Nanoshells and Nanorods, used in this experiment, absorption spectra

2.2 Experimental Setup

Tissue simulating phantoms were used to mimic the scattering and absorption properties of tissue in solution. For the tissue simulating phantom a solution was made using 10% intravenous fat emulsion (Liposyn II 10%, *Abbott Laboratories*, North Chicago, IL) and 90% dH2O. The dilution factor was chosen to give the solution similar scattering and absorption values to human tissue at the wavelength chosen for irradiation.(61) The GNPs were mixed into the tissue phantom solution at multiple concentrations, from 1x – 40x for nanoshells and nanorods, where x is the physiological concentration of nanoshells found in tumors after intravenous inoculation in mice (1.14×10^9 GNPs/mL). (58-59)

These different concentration solutions of GNPs and tissue phantom, including the control with only tissue phantom, were pippetted into 96 well plates (Thermo Fisher Scientific, Inc., Waltham, MA) at a volume of 300 μL each. As shown in the schematic (Figure 4) the 96 well-plate was placed under the thermographic camera, SC4000, (FLIR Sys., Boston, MA) with the laser light irradiating the sample from a slight angle. The laser used in this setup was an NIR (λ = 800 nm) diode-laser (Opto Power Corp., Tucson, AZ) with a diode-laser controller (Opto Power Corp.) that allowed for pulsed irradiation and a power up to 5 W.

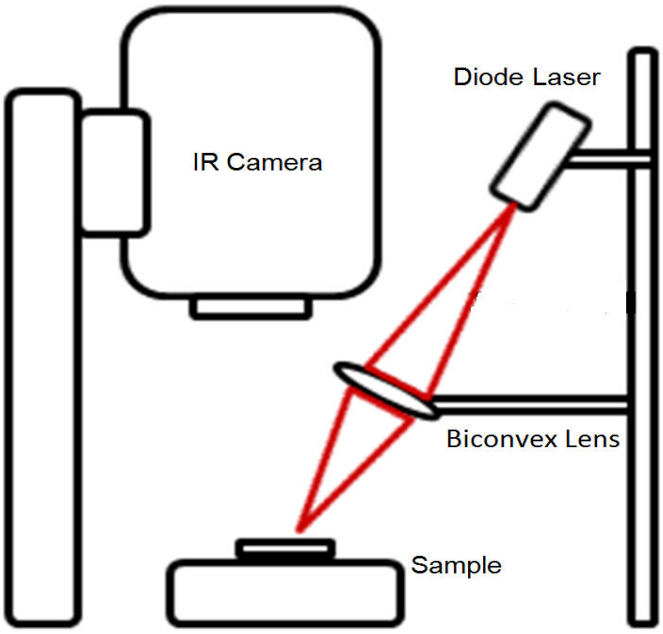

Figure 4: Experimental Schematic. Shows sample of GNPs with tissue phantom being irradiated with diode laser at 800 nm, and temperature measured using infrared camera

The laser spot size was focused to approximately 0.4 cm onto each well using a biconvex lens (Newport Corp., Irvine, CA) with a diameter of 50.8 mm and a focal length of 62.9 mm. The laser irradiation was performed at 3 different fluence rates, 3.5 W/cm^2, 4 W/cm^2 (due to their use in prior *in vitro* experiments) and 1.75 W/cm^2 as a lower threshold to compare against. (20) To confirm the laser power transmitted into the solution a power meter (Newport Corp.) was used prior to each experiment.

2.3 Data Analysis

Using the ThermoVision software (FLIR Sys., Boston, MA) in conjunction with the IR camera, the region of interest – the center of the laser spot – was selected and the

temperature was measured during the time of laser irradiation, ranging from 1-100 seconds. The temperature versus time data was extracted for all concentrations, fluence rates and each GNP. The plastic surroundings insulated and forced the heat to be confined within the volume adding on to the photothermal effect of the GNPs. Thus, all temperature data was taken during 1 second exposure, which allows an accurate evaluation the dynamics of only the GNP system. This can be done because during this time period there is no diffusion throughout the system. All comparisons and analyses were performed in MATLAB (The Mathworks Inc., Natick, MA).

2.4 Nanoparticle Simulations

To determine the absorption and scattering properties of these nanoshells and nanorods, electromagnetic simulations were performed. Simulations of the nanorod heating were performed in a Discrete Dipole Approximation (DDA) program (DDSCAT 6.1) to compare with experimentation.(62) DDA can simulate the nanorod scattering and absorption in different orientations and at different incident polarizations. For DDA simulations, the chosen shape to accurately represent the nanorod was the cylinder with hemispherical caps. The aspect ratio and geometric properties were determined using the known length and width from the TEM data.(56-57)

Using Maetzler's Mie Theory Code, an exact solution for Maxwell's equations for coated spheres, nanoshell heating was simulated.(63) In this case, the TEM derived nanoshell size was inputted along with the dielectric functions for the inner sphere of silica as well as the outer shell of gold. The nanoshell scattering and absorption

components were obtained using the program to show the ratio between the two components. The dielectric function for bulk gold, determined by Johnson and Christy, was used for both nanoshell and nanorod simulations.(64)

The theoretical absorption values for both nanorods and nanoshells were used to determine the concentrations for both GNPs to achieve the equivalent change in temperature. To model the experimental data, a Monte Carlo method, using code written by Wang and Jacques, was utilized, in which the program simulates the given sample with thousands of individual photons and averages over all simulated values.(65) The specific data determined was the expected power that was absorbed from the laser irradiation onto the sample. To simulate this sample, the input included the measured absorption coefficient (μ_a), scattering coefficient (μ_s), anisotropy (g), and power of the laser. This expected power absorbed was used to determine the expected change in temperature for the solution using a finite difference model (FDM) based on the General Heat Transfer Equation:

$$\rho_t c \frac{\partial T}{\partial t} = \nabla \cdot (k \nabla T) + Q_{gen} \quad (1)$$

In this equation, ρ_t is the density of solution (1000 kg/m^3), c is the specific heat capacity (3800 J/(kg*K)), k is the thermal conductivity (0.6 W/(m*K)), and Q_{gen} is the heat generated from a source within the tissue, determined using Monte Carlo. The details of the derivation are shown in the Appendix.

These governing equations were then coded into MATLAB, taking the inputted generated heat from the Monte Carlo code and converting this into a temperature profile

with respect to time and depth (Appendix). By changing the μ_a values, in the Monte Carlo method, based on the concentration of GNPs in solution, the expected change in temperature was rendered equivalent to the experimental change in temperature. Thus, the change in temperature of the sample was estimated, such that it could be compared to the experimental analysis as shown in the results.

RESULTS

3.1 Temperature Increase of Nanoparticles:

In Figure 5, it is explicitly seen that the GNPs both increase in temperature over time. Additionally with increasing concentration the GNPs increase in temperature. In comparison to the control experiment, when the tissue simulating phantom was irradiated with the laser, the nanorods (Figure 5a) and nanoshells (Figure 5b) both had significantly higher temperatures. All of these properties are seen in photothermal probes and confirms that these nanoparticles are photothermally active.

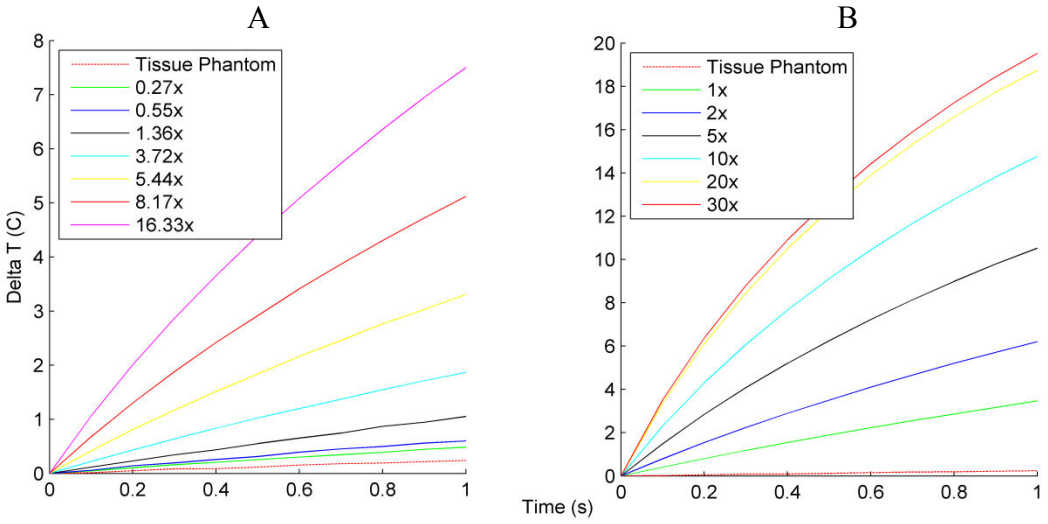

Figure 5: Increase in temperature over time. (A) Nanorod increase in temperature with increasing concentrations (x = 1.14 x 10^9) over 1 second exposure at 3.5 W/cm^2, (B) Nanoshells increase in temperature with increasing concentrations over 1 second exposure at 3.5 W/cm^2

Both of these particles seem to have a high enough increase in temperature to move from body temperature of 37°C to the hyperthermia targeted temperature to cause protein denaturation and thermal damage (~ 45°C). Therefore, it is apparent that these

particles can be used for photothermal therapy. However, it is also apparent that the change in temperature for nanorods is much lower than the nanoshell change in temperature.

There is a significant difference between the two particles, as shown in Figure 6, when comparing the change in temperature of nanoshells versus nanorods.

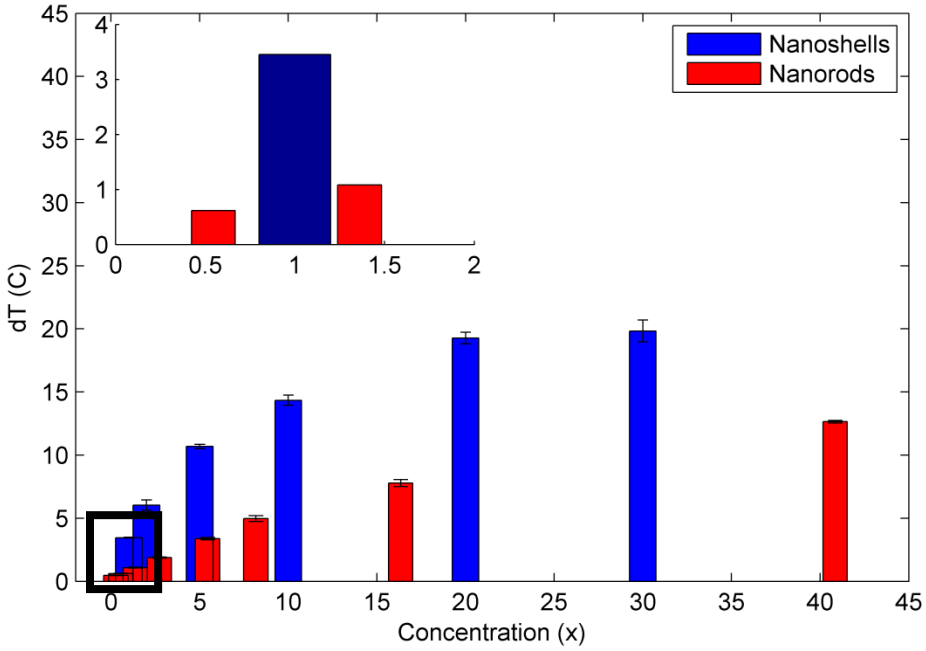

Figure 6: Increase in temperature over 1 second. Bar plot showing the temperature increase with respect to concentration of nanoshells and nanorods over a one second exposure. Inset shows zoomed in view for comparison of nanoshell and nanorod increase in temperature around 1x concentration. Error bars are standard deviation over multiple trials.

For nanoshells (Figure 6) with increasing concentrations the change in temperature increased significantly up to around 20 °C in 1 second, showing that the particle is effective in converting the light into heat. The nanorods had a much smaller

increase in temperature for the same concentrations as nanoshells due to their smaller absorption cross-section, but the same increasing trend is visible, confirming the photothermal nature of these particles. The inset in Figure 6 zooms in on the temperature increase around the 1x concentration of nanoshells and nanorods. As can be seen in this plot, the nanoshell change in temperature at 1x is much greater than (around 3.5 times) the nanorod change in temperature at 0.55x and 1.33x concentrations. This confirms the hypothesis that the nanoshells generate more heat on a per particle basis, due to their higher absorption cross-section. This is an important point to consider when choosing nanoparticle probes for photothermal therapy.

3.2 Mie Theory Simulation

Mie Theory and DDA simulations were performed to determine the absorption efficiencies of nanoshells and nanorods, using the dimensions extracted from the TEM images. The optical properties of both particles are accurately determined using both of these simulations. From Mie Theory, it is shown (Figure 7) that the nanoshell absorption efficiency (approximately 2), at the peak, is approximately 1/5 of the total extinction whereas scattering results in 4/5 of the total extinction. Therefore to adjust for the large scattering component, the extinction data must always be reduced by a fact of 1/5 to determine the absorption.

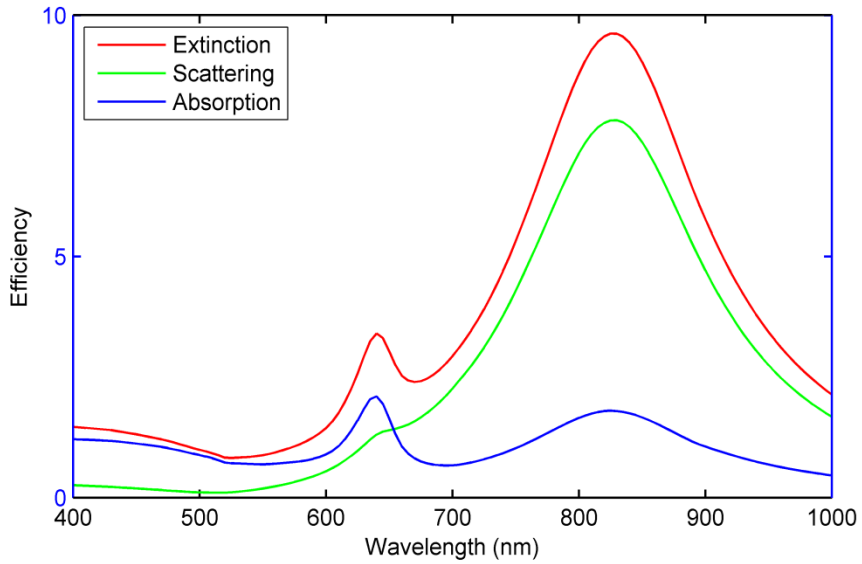

Figure 7: Mie Simulations of Nanoshells. Nanoshell simulated extinction, scattering and absorption efficiency with respect to wavelength.

The absorption efficiency for nanoshells is much larger than for natural chromophores and nanoshells still have a much larger absorption cross-section than most photothermal probes. This large scattering component was expected due to the larger relative size of the nanoshells. Additionally, it is evident that the large absorption cross-section of nanoshells is due to the large size and not due to the relatively low absorption efficiency.

3.3 Discrete Dipole Approximation Simulation

DDA simulations were also completed to show that the absorption efficiency of nanorods is orientation dependent (Figure 8b). As the different angles (orientation) are varied the absorption changes dramatically. The maximum absorption (approximately 18, shown in Figure 8a) is when the nanorod is oriented in the same plane as the

polarization of the electric field (φ = 0°, θ = 90° in inset of Figure 8a) as earlier discussed, and the minimum absorption is whenever the nanorod is perpendicular to the polarization direction (most apparent at φ = 90° and θ is any value). The average absorption efficiency (approximately 12) is determined by averaging over all φ and θ and is shown in comparison to the maximum absorption efficiency in Figure 9a. This value for average (adjusted) absorption efficiency is equivalent to a randomly oriented solution of nanorods.

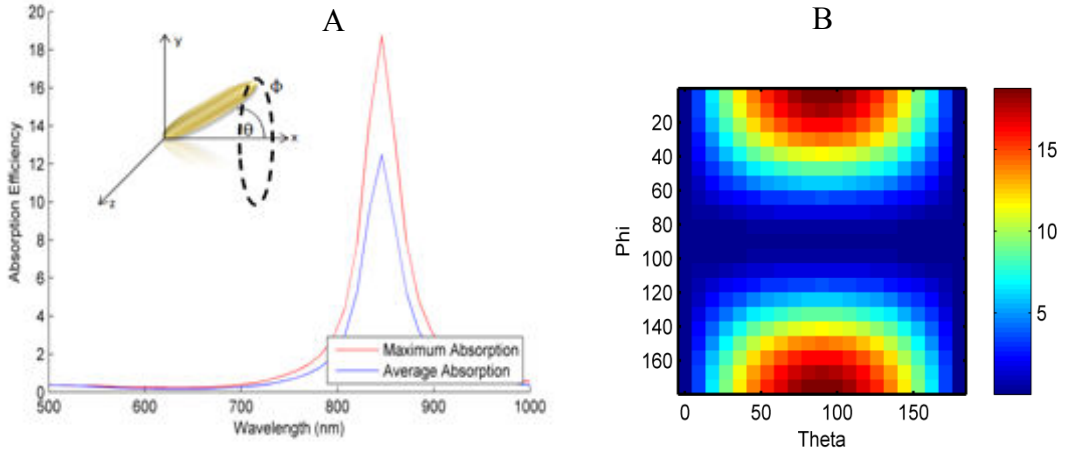

Figure 8: Simulated Absorption Efficiency of Nanorods. (A) Shows the maximum and average (adjusted) absorption efficiency of nanorods using DDA, inset shows the orientation and specifies the angles φ and θ. (B) Shows how the nanorod absorption changes as the values of φ and θ change.

In the solutions for this experiment, the nanorods were randomly oriented; therefore this will give a good approximation for the solutions used in this experiment. Additionally, in photothermal therapy *in vitro* and *in vivo,* the nanorods will also be randomly oriented since there is no efficient to orient nanorods in solution, so this value

will again be a good approximation for this case. The nanorod average optical absorption efficiency is shown to be much larger than the nanoshell optical absorption efficiency (approximately a factor of 6). Therefore the nanorods are more efficient at optically absorbing light, per particle, than the nanoshells, which is another important point to consider in the choice of particle for photothermal therapy. These adjusted values of the absorption efficiencies, determined using both nanoparticle simulations, were used to resolve the theoretical temperature increase to compare against the experimental values using Monte Carlo and Finite Difference Modeling.

3.4 Concentration Equivalence Factor for Nanoshells and Nanorods

To determine the respective concentrations at which the nanorods and nanoshells have equivalent heating the ratio between the heating of fixed nanoshell concentration (1x, 2x, 5x) and varying concentrations of nanorods was plotted versus nanorod concentration (Figure 9). The plot of the ratio was created using an interpolation that simulated the values in between the known points. By looking at Figure 9, it is apparent that the point where the ratio is equal to 1 was when the concentration of nanorods was approximately 5.5 times the fixed concentration of the nanoshells.

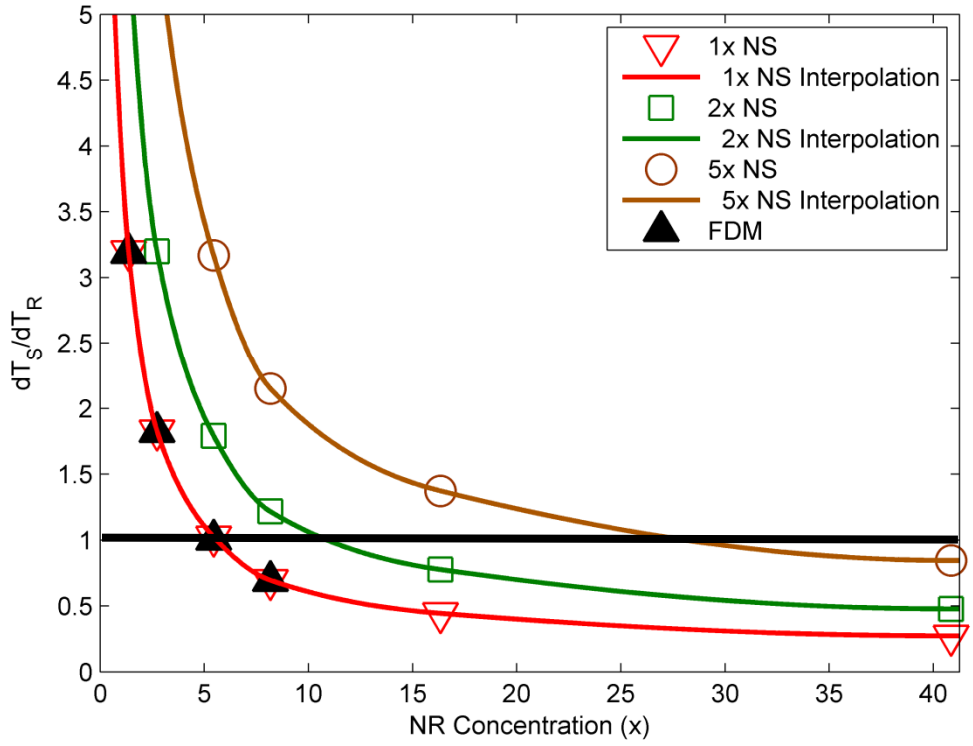

Figure 9: Concentration Equivalence of Nanoparticles. This plot shows the ratio of change in temperature of a constant nanoshell concentration and the change in temperature for varying concentration of nanorods (x-axis) for a fluence rate of 3.5 W/cm^2. Nanorods and nanoshells have the same generated heat when the ratio is equal to one (black line).

In Figure 9, for the 1x constant nanoshell concentration, the ratio is equal to one at a nanorod concentration of 5.5, for 2x nanoshell concentration, the ratio is equal to one at around 11x nanorod concentration and finally for 5x nanoshell concentration, the ratio is equal to one at around 28x nanorod concentration. Additionally, using the obtained theoretical absorption properties and the Monte Carlo and Finite Difference Modeling (FDM), the same ratio for the constant 1x nanoshells concentration case was modeled.

This FDM data follows the same general trend as the experimental data (black triangles in Figure 9) that the nanorod concentration is 5.5 times the nanoshell concentration. Furthermore, the same trend is followed for all the fluence rates explored in the experiment and in the FDM (data not shown). This result is the concentration of nanorods at which they generate the same heat as nanoshells was one of the primary goals of this study. The concentration equivalence is important because it gives a numerical value (5.5) to the number of nanorods that needs to reach the tumor site *in vivo* to generate the same amount of heat for nanoshells.

DISCUSSION

This study was based on the known physiological dose of nanoshells that reach the tumor site *in vivo*. The heat generated by this concentration of nanoshells has been shown to be enough to cause cell death and a significant reduction in tumor size. In current literature, the same value is unknown for nanorods. As a result, the heat generation based on the physiologic does of nanoshells, was the chosen as the low end threshold, for determining the equivalent concentration of nanorods necessary to cause tumor ablation. As this study has shown, to achieve similar values in heat generation it is necessary to have 5.5 times the concentration nanorods as the concentration of nanoshells, for these specific sizes of nanoshells and nanorods. However, this can be estimated for other sizes of particles using the DDA and Mie approach detailed above, which is shown to be accurate compared to experimental values (Figure 9).

Due to their higher absorption cross-section the nanoshells have a much higher heat generation per particle, as discussed earlier. At a preliminary glance, nanoshells seem to be a better nanoparticle. However, there is more to take into account than the absorption cross-section; the size of the GNPs, for one, which corresponds to a high scattering component in nanoshells and could be construed as useful or not. Also an important point is that the optical absorption efficiency of nanorods is much higher. There could be differences in the geometry between particles and within solutions of the same particles leading to possible increases and decreases in absorption. The distribution of the metal around the surface of the GNP can affect these optical properties, including

elongation/compression of the particle and surface roughness. Finally, there could be thermal issues within the solution during heating. Since the temperature at the surface of the GNP cannot be determined, it is possible that there are heating effects in the direct surroundings of the GNPs. This includes such possibilities, since the temperatures within the solution are most likely reaching boiling point temperatures, as vaporization and localized evaporation of the water, which can cause steam pockets and cavitation bubbles. These steam pockets and cavitation bubbles may affect the optical properties of the surrounding nanorods and nanoshells due to the refractive index changes that are not taken into account in the experiment.

Using DDA and Mie Theory, it is shown in Table 1, how this can be generalized for many different sized nanoparticles. In this table, the factor is shown that is necessary to determine the amount of nanorods that generates the same heat with nanoshells, as previously discussed. The table consists of four common NIR nanorods, with an aspect ratio of 3.9, and three common NIR nanoshells, with a R_1/R_2 ratio of 0.856.(38)

	NR 1	NR 2	NR 3	NR 4
NS 1	11.61	5.63	2.21	1.6
NS 2	20.28	9.83	3.87	2.79
NS 3	31.19	15.11	5.95	4.28

Table 1: Nanorod Concentration Necessary for Equivalent ΔT. This factor is shown for commonly used photothermal nanorod dimensions with a constant aspect ratio of 3.9 (thus, NIR absorption) NR 1: $R_{effective}$ = 8.74 nm, NR 2: $R_{effective}$ = 11.43 nm, NR 3: $R_{effective}$ = 17.9 nm, and NR 4: $R_{effective}$ = 21.86 nm. Commonly used photothermal nanoshell dimensions with a constant ratio R_1/R_2 (inner to outer radius) of 0.856, thus NIR absorption. NS 1: R_2 = 70 nm; NS 2: R_2 = 105 nm; NS 3: R_2 = 140 nm.

The wide variety of sizes in the table shows how the factor changes within typical nanorod and nanoshell sizes for photothermal therapy *in vivo*. For nanoshells, the absorption component was determined to much lower than the scattering component, and as a result the absorption had to be calculation for absorption of nanoshells had to be adjusted. To determine the absorption for the randomly oriented solution of nanorods it was necessary to average the absorption efficiency for all possible orientations.

Finally, since the targeting efficiency of nanorods is not completely certain, it is possible that at similar doses to nanoshells, more particles can reach the tumor site. Effectively, if nanorods can reach the tumor site at a rate of 5.5 times more than nanoshells then this would negate the lower heat generation and it would be more efficient in converting the available laser power into heat. The choice of GNP may even be an application dependent process based on whether it was necessary to have smaller GNPs to reach a targeted site or more heating with fewer particles. This study, effectively, is successful in determining the concentration equivalency factor between nanoshells and nanorods for achieving similar heating as well as the ability of both GNPs to convert light into heat. This gives a basis for deciding which plasmonic GNP to use in future experiments and clinical trials using GNP mediated photothermal therapies in ablating cancerous tumors.

CONCLUSION

Overall, in this experiment the determination of the GNP of choice for photothermal therapy is now clearer, however, it is still not a straightforward choice. In this study, using Mie Theory and DDA to simulate the nanoparticle optical properties, it was determined that the average adjusted optical absorption efficiency for nanorods is much higher (six-fold) than the adjusted optical absorption efficiency for nanoshells per particle. Yet due to the larger size of nanoshells, their absorption cross-section is much larger than nanorods. This is shown explicitly in the simple temperature increase plots (Figures 5 and 6) by the nanoshells having a much larger increase in temperature than the nanorods of similar concentrations, thus saying that nanoshells have a higher increase in temperature per particle. Additionally, in Figure 9, it is shown that to reach the same generated heat, it is necessary to have 5.5 times the concentration of nanoshells for nanorods, for these GNP sizes.

In this case, both GNPs have uses in photothermal therapy depending on the targeting efficiency of nanorods versus nanoshells. If the targeting efficiency for nanorods is 5.5 times of greater than nanoshells, for this size, nanorods should likely be the choice of GNP, but if there is an application in which there is a limited volume or limited number of GNPs that are used, then nanoshells should be chosen for photothermal therapy. Therefore, with this information, an educated choice can be determined on which GNP to use for photothermal therapy based on the application.

APPENDIX

Finite Difference Derivation and Code:

A convection boundary was included for the modeling the surface of the GNP phantom:

$$k\left[\frac{\partial T}{\partial n}\right]_s = h(T_s - T_\infty) \quad (1)$$

Such that in this equation h is the convection heat transfer coefficient and T_s is the surface temperature and T_∞ is the environment temperature. Next, all spatial and time derivatives are converted into approximately equivalent difference quotients based on Taylor's Theorem, which is used to derive the Central Difference Theorem (shown for first spatial derivative):

$$\frac{\delta T(x,z,t)}{\delta z} = \frac{T^m{}_{i+1,k} - T^m{}_{i-1,k}}{2\Delta z} \quad (2)$$

where the i, k, and m are the x, z, and t components. Using these conversions, the governing equations for each node were determined for the FDM.

```
%% Input from Monte Carlo Code
NS_1=dlmread('NS.Arzc','\t',1,0);

%% Heating Parameters with meters
Cp_gold = 129;     % [J/kg*K]
rho_gold = 1932;   % [kg/m^3]
Cp_tp = 3800;      % [J/kg*K] tissue phantom
rho_tp = 1000;     % [kg/m^3] tissue phantom
geo_cross_sec_measured_NR = pi*(8.712e-7)^2;
geo_cross_sec_measured_NS = pi*(62.5e-7)^2;
fluence_05 = 1.75*sec;  %J/cm^2
fluence_1 = 3.5*sec;    %J/cm^2
%% Parameters
sec = 1;           % Max time
```

```
tau_C = 1;          % Laser Pulse Duration
k = 0.6;            % [W/m*C] thermal conductivity for tissue phantom
h = 3;              % [W/m^2*C]
T_init = NS_1(1,3);     % Initial Temperature [C]
t_room = T_init;  % Room Temp [C]
Cp_Rho = Cp_h2o*rho_h2o;
i = 0;              % z counter [m]
t_c = 0;            % Time counter [s]
lambda = 800e-9;  % Wavelength [m]
del_t = 0.0017;   % Time step size [s]
del_z = 2e-4;     % Depth step size [m]
B = (h*del_z)/k;  % Biot Number
alpha = k/(Cp_Rho);
Fz = (alpha*del_t)/((del_z)^2);     % Fourier Coeff. Stability Crit.
S = ((NS_1(:,3))).*100^3;     % Source Term [W/m^3]
time = 0:del_t:sec;     % Time Duration
z = del_z:del_z:1e-2;   % Depth Duration

%% Finite Difference Model
clear temp
temp = zeros(1e-2/del_z,round(sec/del_t));      % Initialize Temp
for j = 1:1:length(time)      % Total Time Period
    for i = 1:1:length(z)     % Total Depth
        if (time(j) == 0)     % Initialize Temp
            temp(i,j) = T_init;
        elseif(i > 1 && i < length(z))    % If within sample
            if (time(j) > tau_C)          % If outside of laser pulse
                temp(i,j) = (Fz*(temp(i+1,j-1)+temp(i-1,j-
1)))+(temp(i,j-1)*(1-(2*Fz)));
            else
                temp(i,j) = (Fz*(temp(i+1,j-1)+temp(i-1,j-
1)))+(temp(i,j-1)*(1-(2*Fz)))+((S(i)*del_t)/(Cp_Rho));
            end
        elseif (i == 1) % If at surface
            if (time(j) > tau_C)    % If outside of laser pulse
                temp(i,j) = (2*Fz*(temp(i+1,j-
1)+(B*t_room)))+(temp(i,j-1)*(1-(2*Fz)-(2*B*Fz)));
            else
                temp(i,j) = (2*Fz*(temp(i+1,j-
1)+(B*t_room)))+(temp(i,j-1)*(1-(2*Fz)-
(2*B*Fz)))+((S(i)*del_t)/(Cp_Rho));
            end
        elseif (i == length(z))     % If at bottom of sample
            if (time(j) > tau_C)    % If outside of laser pulse
                temp(i,j) = (2*Fz*temp(i-1,j-1))+(temp(i,j-1)*(1-
(2*Fz)));
            else
                temp(i,j) = (2*Fz*temp(i-1,j-1))+(temp(i,j-1)*(1-
(2*Fz)))+((S(i)*del_t)/(Cp_Rho));
            end   end   end   end
```

REFERENCES

1. Jemal A, Siegel R, Ward E, Hao YP, Xu JQ, Thun MJ. Cancer Statistics, 2009. Ca-a Cancer Journal for Clinicians 2009; 59(4):225-249.

2. Boyle PCL, B. World Cancer Report. Geneva: World Health Organization; 2008. 512 p.

3. Hanahan D, Weinberg RA. The hallmarks of cancer. Cell 2000; 100(1):57-70.

4. Frei III E AK. Principles of Dose, Schedule, and Combination Chemotherapy. In: al Be, ed. Cancer Medicine. Hamilton, Ontario: BCDecker. 2000.

5. Mundt A RJ, Weichselbaum R. Physical and Biologic Basis of Radiation Oncology. In: al Be, ed. Cancer Medicine. Hamilton, Ontario: BCDecker. 2000.

6. Pollock R MD. Principles of Surgical Oncology. In: al Be, ed. Cancer Medicine. Hamilton, Ontario: BCDecker. 2000.

7. V BB. Thermal potentiation of mammalian cell killing: Clues for understanding and potential for tumor therapy. Adv Radiat Biol 1976; 6:267-324.

8. Henle KJ, Dethlefsen LA. HEAT FRACTIONATION AND THERMOTOLERANCE - REVIEW. Cancer Research 1978; 38(7):1843-1851.

9. Hobbs SK, Monsky WL, Yuan F, Roberts WG, Griffith L, Torchilin VP, Jain RK. Regulation of transport pathways in tumor vessels: Role of tumor type and microenvironment. Proceedings of the National Academy of Sciences of the United States of America 1998; 95(8):4607-4612.

10. Lepock JR. Cellular effects of hyperthermia: relevance to the minimum dose for thermal damage. Int J Hyperthermia 2003; 19(3):252-266.

11. Laszlo A. The effects of hyperthermia on mammalian cell structure and function. Cell Prolif 1992; 25:59-87.

12. Goldberg SN. Radiofrequency tumor ablation: principles and techniques. Eur J Ultrasound 2001; 13(2):129-147.

13. Mirza AN, Fornage BD, Sneige N, Kuerer HM, Newman LA, Ames FC, Singletary SE. Radiofrequency ablation of solid tumors. Cancer Journal 2001; 7(2):95-102.

14. Sato M, Watanabe Y, Ueda S, Iseki S, Abe Y, Sato N, Kimura S, Okubo K, Onji M. Microwave coagulation therapy for hepatocellular carcinoma. Gastroenterology 1996; 110(5):1507-1514.

15. Kremkau FW. CANCER-THERAPY WITH ULTRASOUND - HISTORICAL REVIEW. Journal of Clinical Ultrasound 1979; 7(4):287-300.

16. Steeves RA. HYPERTHERMIA IN CANCER-THERAPY - WHERE ARE WE TODAY AND WHERE ARE WE GOING. Bulletin of the New York Academy of Medicine 1992; 68(2):341-350.

17. Welch AJ. THE THERMAL RESPONSE OF LASER IRRADIATED TISSUE. Ieee Journal of Quantum Electronics 1984; 20(12):1471-1481.

18. Anderson RR, Parrish JA. Microvasculature can be selectively damaged using dye lasers: a basic theory and experimental evidence in human skin. Lasers Surg Med 1981; 1(3):263-276.

19. Chen WR, Adams RL, Bartels KE, Nordquist RE. CHROMOPHORE-ENHANCED IN-VIVO TUMOR-CELL DESTRUCTION USING AN 808-NM DIODE-LASER. Cancer Letters 1995; 94(2):125-131.

20. Hirsch L R SRJ, Bankson J A, Sershen S R, Rivera B, Price R E, Hazle J D, Halas N J, West J L. Nanoshell-mediated near-infrared thermal therapy of tumors under magnetic resonance guidance. PNAS 2003; 100(23):13549-13554.

21. Zharov VP, Galitovskaya EN, Johnson C, Kelly T. Synergistic enhancement of selective nanophotothermolysis with gold nanoclusters: Potential for cancer therapy. Lasers in Surgery and Medicine 2005; 37(3):219-226.

22. Pitsillides CM, Joe EK, Wei XB, Anderson RR, Lin CP. Selective cell targeting with light-absorbing microparticles and nanoparticles. Biophysical Journal 2003; 84(6):4023-4032.

23. Tong L, Zhao Y, Huff TB, Hansen MN, Wei A, Cheng JX. Gold nanorods mediate tumor cell death by compromising membrane integrity. Advanced Materials 2007; 19:3136-+.

24. El-Sayed I H HX, El-Sayed M A. Selective laser photo-thermal therapy of epithelial carcinoma using anti-EGFR antibody conjugated gold nanoparticles. Cancer Letters 2005; 239:129-135.

25. Huang XH, Jain PK, El-Sayed IH, El-Sayed MA. Plasmonic photothermal therapy (PPTT) using gold nanoparticles. Lasers in Medical Science 2008; 23(3):217-228.

26. Gabizon AA. Stealth liposomes and tumor targeting: One step further in the quest for the magic bullet. Clinical Cancer Research 2001; 7(2):223-225.

27. Ferrari M. Cancer nanotechnology: Opportunities and challenges. Nature Reviews Cancer 2005; 5(3):161-171.

28. Peer D, Karp JM, Hong S, FaroKhzad OC, Margalit R, Langer R. Nanocarriers as an emerging platform for cancer therapy. Nature Nanotechnology 2007; 2(12):751-760.

29. Gobin AM, Lee MH, Halas NJ, James WD, Drezek RA, West JL. Near-infrared resonant nanoshells for combined optical imaging and photothermal cancer therapy. Nano Letters 2007; 7(7):1929-1934.

30. Durr NJ, Larson T, Smith DK, Korgel BA, Sokolov K, Ben-Yakar A. Two-photon luminescence imaging of cancer cells using molecularly targeted gold nanorods. Nano Letters 2007; 7(4):941-945.

31. Park J, Estrada A, Sharp K, Sang K, Schwartz JA, Smith DK, Coleman C, Payne JD, Korgel BA, Dunn AK, Tunnell JW. Two-photon-induced photoluminescence imaging of tumors using near-infrared excited gold nanoshells. Optics Express 2008; 16(3):1590-1599.

32. Rhyner MN, Smith AM, Gao XH, Mao H, Yang LL, Nie SM. Quantum dots and multifunctional nanoparticles: new contrast agents for tumor imaging. Nanomedicine 2006; 1(2):209-217.

33. Smith AM, Duan HW, Mohs AM, Nie SM. Bioconjugated quantum dots for in vivo molecular and cellular imaging. Adv Drug Deliv Rev 2008; 60(11):1226-1240.

34. Bulte JWM, Kraitchman DL. Iron oxide MR contrast agents for molecular and cellular imaging. Nmr in Biomedicine 2004; 17(7):484-499.

35. Corot C, Robert P, Idee JM, Port M. Recent advances in iron oxide nanocrystal technology for medical imaging. Adv Drug Deliv Rev 2006; 58(14):1471-1504.

36. Loo C, Lowery A, Halas N, West J, Drezek R. Immunotargeted nanoshells for integrated cancer imaging and therapy. Nano Letters 2005; 5(4):709-711.

37. Jain PK, El-Sayed MA. Plasmonic coupling in noble metal nanostructures. Chemical Physics Letters 2010; 487(4-6):153-164.

38. Jain PK, Lee KS, El-Sayed IH, El-Sayed MA. Calculated absorption and scattering properties of gold nanoparticles of different size, shape, and composition: Applications in biological imaging and biomedicine. Journal of Physical Chemistry B 2006; 110(14):7238-7248.

39. Oldenburg SJ, Averitt RD, Westcott SL, Halas NJ. Nanoengineering of optical resonances. Chemical Physics Letters 1998; 288(2-4):243-247.

40. Aubin-Tam ME, Hwang W, Hamad-Schifferli K. Site-directed nanoparticle labeling of cytochrome c. Proceedings of the National Academy of Sciences of the United States of America 2009; 106(11):4095-4100.

41. Cedervall T, Lynch I, Lindman S, Berggard T, Thulin E, Nilsson H, Dawson KA, Linse S. Understanding the nanoparticle-protein corona using methods to quantify exchange rates and affinities of proteins for nanoparticles. Proceedings of the National Academy of Sciences of the United States of America 2007; 104(7):2050-2055.

42. Liao HW, Hafner JH. Gold nanorod bioconjugates. Chemistry of Materials 2005; 17(18):4636-4641.

43. Kumar S, Aaron J, Sokolov K. Directional conjugation of antibodies to nanoparticles for synthesis of multiplexed optical contrast agents with both delivery and targeting moieties. Nature Protocols 2008; 3(2):314-320.

44. Brannon-Peppas L, Blanchette JO. Nanoparticle and targeted systems for cancer therapy. Adv Drug Deliv Rev 2004; 56(11):1649-1659.

45. He X WWF, Crowe J H, Swanlund D J, Bischof J C. In Situ Thermal Denaturation of Proteins in Dunning AT-1 Prostate Cancer Cells: Implication for Hyperthermic Cell Injury. Annals of Biomedical Engineering 2004; 32(10):1384-1398.

46. Huttmann G, Birngruber R. On the possibility of high-precision photothermal microeffects and the measurement of fast thermal denaturation of proteins. Ieee Journal of Selected Topics in Quantum Electronics 1999; 5(4):954-962.

47. Zharov VP, Galitovsky V, Viegas M. Photothermal detection of local thermal effects during selective nanophotothermolysis. Applied Physics Letters 2003; 83(24):4897-4899.

48. Pustovalov VK, Smetannikov AS, Zharov VP. Photothermal and accompanied phenomena of selective nanophotothermolysis with gold nanoparticles and laser pulses. Laser Physics Letters 2008; 5(11):775-792.

49. Zharov VP, Galitovskaya E, Viegas M. Photothermal guidance for selective photothermolysis with nanoparticles. Laser Interaction with Tissue and Cells Xv 2004; 5319:291-300.

50. O'Neal DP, Hirsch LR, Halas NJ, Payne JD, West JL. Photo-thermal tumor ablation in mice using near infrared-absorbing nanoparticles. Cancer Letters 2004; 209(2):171-176.

51. Huang XH, El-Sayed IH, Qian W, El-Sayed MA. Cancer cell imaging and photothermal therapy in the near-infrared region by using gold nanorods. Journal of the American Chemical Society 2006; 128(6):2115-2120.

52. Dickerson EB, Dreaden EC, Huang XH, El-Sayed IH, Chu HH, Pushpanketh S, McDonald JF, El-Sayed MA. Gold nanorod assisted near-infrared plasmonic photothermal therapy (PPTT) of squamous cell carcinoma in mice. Cancer Letters 2008; 269(1):57-66.

53. Takahashi H, Niidome T, Nariai A, Niidome Y, Yamada S. Gold nanorod-sensitized cell death: Microscopic observation of single living cells irradiated by pulsed near-infrared laser light in the presence of gold nanorods. Chemistry Letters 2006; 35(5):500-501.

54. Takahashi H, Niidome T, Nariai A, Niidome Y, Yamada S. Photothermal reshaping of gold nanorods prevents further cell death. Nanotechnology 2006; 17(17):4431-4435.

55. Lu W, Xiong CY, Zhang GD, Huang Q, Zhang R, Zhang JZ, Li C. Targeted Photothermal Ablation of Murine Melanomas with Melanocyte-Stimulating Hormone Analog-Conjugated Hollow Gold Nanospheres. Clinical Cancer Research 2009; 15(3):876-886.

56. Brioude A, Jiang XC, Pileni MP. Optical properties of gold nanorods: DDA simulations supported by experiments. Journal of Physical Chemistry B 2005; 109(27):13138-13142.

57. Lee KS, El-Sayed MA. Dependence of the enhanced optical scattering efficiency relative to that of absorption for gold metal nanorods on aspect ratio, size, end-cap shape, and medium refractive index. Journal of Physical Chemistry B 2005; 109:20331-20338.

58. Zaman RT, Diagaradjane P, Wang JC, Schwartz J, Rajaram N, Gill-Sharp KL, Cho SH, Rylander HG, Payne JD, Krishnan S, Tunnell JW. In vivo detection of gold nanoshells in tumors using diffuse optical spectroscopy. Ieee Journal of Selected Topics in Quantum Electronics 2007; 13(6):1715-1720.

59. James WD, Hirsch LR, West JL, O'Neal PD, Payne JD. Application of INAA to the build-up and clearance of gold nanoshells in clinical studies in mice. Journal of Radioanalytical and Nuclear Chemistry 2007; 271:455-459.

60. Jana NR, Gearheart L, Murphy CJ. Wet chemical synthesis of high aspect ratio cylindrical gold nanorods. Journal of Physical Chemistry B 2001; 105(19):4065-4067.

61. Vanstaveren HJ, Moes CJM, Vanmarle J, Prahl SA, Vangemert MJC. Light-Scattering In Intralipid-10-Percent In The Wavelength Range Of 400-1100 nm. Applied Optics 1991; 30(31):4507-4514.

62. Draine BT, Flatau PJ. DISCRETE-DIPOLE APPROXIMATION FOR SCATTERING CALCULATIONS. Journal of the Optical Society of America a-Optics Image Science and Vision 1994; 11(4):1491-1499.

63. Matzler C. MATLAB Functions for Mie Scattering and Absorption. Germany Institute of Applied Physics, University of Bern; 2002 June 2002. Report nr 2002-08. 20 p.

64. Johnson PB, Christy RW. OPTICAL-CONSTANTS OF NOBLE-METALS. Physical Review B 1972; 6(12):4370-4379.

65. Wang LH, Jacques SL, Zheng LQ. MCML - Monte-Carlo Modeling Of Light Transport In Multilayered Tissues. Computer Methods and Programs in Biomedicine 1995; 47(2):131-146.

VITA

The author, Varun Pattani, was born in Vancouver, Canada to Paresh and Kalyani Pattani as they were working towards their respective degrees at UBC. After one year, Varun moved with his family to Austin, TX where he stayed for two years until his family moved to The Woodlands, TX where he lived for 13 years. He attended Elementary and Middle School at The John Cooper School and high school, for half a year, at a magnet school, the Academy of Science and Technology. In 2001, he moved with his family to Beaverton, OR and continued his high school career at a magnet school, the School of Science and Technology. Through his success in high school, the author attended Cornell University in Ithaca, NY where he obtained an Electrical and Computer Engineering degree in May of 2008. During the summers of his undergraduate degree, the author had positions in research in BME at the Oregon Health Sciences University working for Dr. Tania Vu and in industry at Intel, Corp working in the chip architecture design team. After his undergraduate degree, the author joined the University of Texas at Austin in Biomedical Engineering for his M.S.E. degree. The author will continue at UT pursuing his Ph.D. while conducting research for his advisor, Dr. James Tunnell.

Permanent address:
Varun Pattani
8676 SW Muledeer Dr.
Beaverton, OR 97007

This thesis was typed by Varun Pattani.